TEMPERATURE PROFILING AT SOUTHERN LATITUDES BY DEPLOYING MICROWAVE RADIOMETER

A.K.Pradhan[1], S. Mondal[2], L.A.T.Machado[3] and P.K.Karmakar[4]
[1]Department of Electronic Science, AcharyaPrafullaChandraCollege, New Barrackpore, North 24 Parganas, Kolkata 700 131, India.
[2]Dumkal Institute of Engineering and Technology, P.O-Basantapur, Dist- Murshidabad, India
[3]Instituto Nacional de Pesquisas Espaciais (INPE) Previsão de Tempo e Estudos Climáticos, CPTEC Road, Cachoeira Paulista, SP, 12630000, Brazil.
[4]Institute of Radiophysics and Electronics, University of Calcutta, Kolkata 700 009, India

ABSTRACT
Multifrequency Microwave Radiometer (MP3000A) from Radiometrics Corporation is deployed at different places of Southern latitude for the profiling of one of thermodynamic variables like Temperature. The radiative intensity down- welling from the atmosphere and is expressed in an equivalent brightness temperature T_b*. The radiation is a nonlinear function of the required quantities and we linearise the expression around a suitably chosen first guess, such as a climatological mean. We describe changes in the brightness temperature around the first guess by means of a weighting function which expresses the sensitivity of* T_b *to the variation of the humidity* $\Delta\rho(h)$ *or the temperature* $\Delta T(h)$ *around their initial values. The variation of brightness temperature with height occurs at 51 – 53 GHz is observed but on the other hand the constancy of brightness temperature with height at 56 – 57 GHz is noticeable. This suggests that the measurement of temperature at a certain place by a ground based radiometer may provide good result by exploiting the 56 – 57 GHz band. In this band we have used four frequencies for the purpose. But to extend our study we have also made an attempt to retrieve the temperature profiles in 51 – 53 GHz band. The retrieval process starts with the calculations of* S_g *and* S_ϵ *for two sub-ensembles of radiometric observations separately. Here* $\boldsymbol{S_g = \langle gg' \rangle}$ *and* $\boldsymbol{S_\epsilon = \langle \epsilon\epsilon' \rangle}$*. The measured brightness temperatures at eight specified channel frequencies at Fortaleza, Brazil on 11th April, 2011 at 05:39 and 17:36 UTC are as shown in table 2. The summery of measured brightness temperature in oxygen band at Belem, Brazil on 26th June, 2011 at 05:30 UTC and on 17th June, 2011 at 17:33 UTC and also at Alcantara, Brazil on 12th March, 2010 at 06:03 UTC and on 15th March, 2010 at 17:57 UTC.*

KEYWORDS: *Microwave Radiometer, Temperature profile, Optimal Estimation, Inversion, Brightness Temperature.*

I. INTRODUCTION

Till date the radiosonde observations (RAOBs) are the fundamental method for atmospheric temperature, wind, and water vapour measurement, in spite of their inaccuracies, cost, sparse temporal sampling and logistic difficulties [1]. A better technology has been sought for decades, but until now, no accurate continuous all weather technology has been demonstrated. The highly stable multichannel radiometer (MP3000A :Radiometrics Corporation, USA) has the capability of producing temperature and water vapour profiles ([2]; [3]; [4]; [1]; [5]; [6]; [7]; [8]) within the admissible accuracies.
Applications for this passive radiometric profiling include: weather forecasting and now casting; detection of aircraft icing and other aviation related meteorological hazards; refractivity profiles; corrections needed for radio-astronomical studies; satellite positioning and GPS measurements; atmospheric radiation fluxes; measurement of water vapour density and temperature as they affect hygroscopic aerosols and smokes.

The present studies of temperature profiling are in the scope of CHUVA project (Cloud processes of the main precipitation systems in Brazil: A contribution to cloud resolving modelling and to the Global Precipitation Measurement). It aims to investigate the different precipitation regimes in Brazil in order to improve remote sensing precipitation estimation, rainfall ground validation and microphysical parameterizations of the tri-dimensional characteristics of the precipitating clouds. Clouds play a critical role in Earth's weather and climate, but the lack of understanding of clouds has been long limited scientists' ability of making accurate predictions about weather and climate change. Climate simulations are sensitive to parameterizations of deep convective processes in the atmosphere. The weather and climate modelling is improving space and time resolution and to accomplish this it is necessary to move from cloud parameterization to explicit microphysical description inside the cloud. Therefore, to improve space-time resolution reducing climate model uncertainties is necessary to better understand the cloud processes. A3-D microphysical processes description of the main precipitating system in Brazil can strongly contributes to this matter and thus will be one of the tasks of the project. Keeping these in view the present authors are intending to get the temperature profile at three different locations and they are: a) Fortaleza (3^0S; 38^0W),b)Belem (1.46^0 S; 48.48^0W) and c) Alcantara (2.4^0S; 44.4^0W) in Brazil by exploiting the ground based radiometric brightness temperatures at desired frequencies. It is to be mentioned here that these locations are urban coastal city in the north-east of Brazil characterized by tropical climate, which according to Köppen classification is the type as Equatorial - summer dry. Rainfall and wind regime are governed mainly by the meridional shift of Inter-tropical Convergence Zone (ITCZ). The ITCZ is located in its northernmost position, normally from August to October, and intense south-easterly winds and low rainfall dominate in the area (dry seasonal). On the other hand, when the ITCZ is in its southernmost position, from March to April, weak south-easterly winds and high rainfall prevail (wet season).

Temperature profiles can be obtained by measuring the radiometric brightness temperature around 60 GHz .Centering this frequency there lies the continuum which we call as oxygen complex band. The opacity is larger near the oxygen feature center, limiting emission observation to several meters in height. Away from the oxygen feature center the opacity is smaller and emission can be observed at increasing height. Since local temperature contributes to emission intensity, temperature profiles can be obtained. In this context it is to be mentioned that in this band the emission is almost dependent on ambient pressure and temperature.

The section III contains the physical principle needed behind the profiling technique. This ultimately culminates to temperature weighting functions at the said three locations. The next section i.e., section IV summarises the basic technique for inverting temperature from the measured radiometric brightness temperatures at or near the oxygen complex. Here, we have chosen the Optimal Estimation Method, in-spite of the in-built facilities available in the radiometer. Incidentally, the inversion depends on the historical background of the chosen parameter of the said location. As the campaign has been performed at three different locations of Brazil it is reasonably taken granted to reconstruct the new background taking help of data taken from BADC (British Atmospheric data Center). This is elaborated in the section V. The results obtained are summarised in section VI and the present work ends with discussions and conclusions in section VII.

II. INSTRUMENT

The The Radiometrics ground based WVP-3000A portable water vapour and temperature profiling radiometer measures the calibrated brightness temperature from which one can derive profiles of temperature, water vapor, and limited resolution profiles of cloud liquid water from the surface to approximately 10 km. The detailed descriptions of the system are given by[1]. A short summary of the instrument characteristics is given here. The noticeable characteristics of the system include a very stable local oscillator, an economical way to generate multiple frequencies and the multi-frequency scanning capability ([5]). The radiometer system consists of two separate subsystems in the same cabinet which shares the same antenna and antenna pointing system. A highly stable synthesizer act as local oscillator and allows tuning to a large number of frequencies within the receiver bandwidth. The water vapour profiling subsystem receives thermal emission at five selected frequencies within 22 – 30 GHz [9]. The temperature profiling subsystem measures sky brightness

temperature within 51-59 GHz. An inbuilt infrared thermometer is provided with the said radiometer to observe the presence of cloud and also measures the cloud base height [10]. Here in this paper, we will restrict ourselves only to derive the temperature profiles at different places of Southern latitude as mentioned earlier, under a collaborative CHUVA Project implemented at Instituto Nacional de Pesquisas Espaciais - INPE, Brazil, at an initial stage. The salient characteristics of the radiometer are shown in Table 1.

Table 1. Characteristics of the Radiometer

Frequencies(GHz) for water vapor and liquid water profiling	22.234,23.035,23.835,26.235,30.00
Frequencies(GHz) for temperature profiling	51.248, 51.76, 52.280, 52.804, 56.02, 56.66, 57.288, 57.964
Absolute accuracy(K)	0.5
Sensitivity(K)	0.25
FWHP bandwidth(deg)	2.2 – 2.4
Gain (dB)	36 - 37
Side lobes(dB)	< - 26

III. GENERAL PHYSICAL PRINCIPLE

The scalar form of Radiative Transfer Equation is remarkably simple in Rayleigh-Jeans limit and is considered to be sufficient to the large majority of microwave applications. The radiative intensity down- welling from the atmosphere and expressed in an equivalent brightness temperature T_b can be written as ([11])

$$T_b = T_{bg} exp\left\{-\int_0^{\infty} \alpha(h')dh'\right\} \int_0^{\infty} T(h)\alpha(h) exp\left\{-\int_0^{h} \alpha(h')dh'\right\} dh \quad (1)$$

Here, T_{bg} is the cosmic background radiation. The attenuation coefficient α is a function of different meteorological parameters.

The radiation is a nonlinear function of the required quantities and we linearise the expression around a suitably chosen first guess, such as a climatological mean. We describe changes in the brightness temperature around the first guess by means of a weighting function which expresses the sensitivity of T_b to the variation of the humidity $\Delta\rho(h)$ or the temperature $\Delta T(h)$ around their initial values

$$\Delta T_b = \int_0^{\infty} [W_\rho(h,f,\theta)\delta\rho(h) + W_T(h,f,\theta)\delta T(h) + W_L(h,f,\theta)\delta L(h) + W_p(h,f,\theta)\delta P(h)]dh \quad (2)$$

for a certain frequency f and elevation angle θ. Here, ρ stands for water vapour, T for temperature, L for liquid water and P for ambient atmospheric pressure respectively. However, the weighting function analyses for humidity W_ρ and temperature W_T by ([12]) showed that the temperature weighing function is given by

$$W_T(h) = \alpha(h)e^{-\tau(0,h)} + e^{-\tau(0,h)} \frac{\partial\alpha(h)}{\partial T} [T(h) - T_{bg}e^{-\tau(h,\infty)} - \int_h^{\infty} T(h')\alpha(h')e^{-\tau(h,h')} dh'] \quad (3)$$

To explain more clearly about the weighting function, we take the temperature weighting function (km^{-1}). If we have a $\delta T(K)$ change in T over a height interval δh (km), the brightness temperature response $\delta T_b(K)$ to this change is $\overline{W}_T \delta T \delta h$ where $\overline{W}_T$ is called the height average of W_T over the height interval δh. The weighting functions are determined from the height profile of attenuation coefficients at different frequencies. However equation (1) and its Rayleigh-Jeans approximation are well discussed by [13] and its more general form including scattering is discussed by [14].

Information on meteorological variables may be obtained from measurements of radiometric brightness temperature T_b as a function of f and/or θ. Equation (1) is used: a) in forward model studies in which the relevant meteorological variables are obtained by radiosonde sounding, b) in inverse problem and parameter retrieval applications in which meteorological information is inferred from measurements from radiometric brightness temperature T_b , c) in system modelling studies in

determining the effects of instrument noise on retrieval and optimum measurement ordinates such as f and/or θ ([15]).

However, for the sake of clarity the temperature weighting function at Fortaleza, Belem, and Aclantara, Brazil is shown in Figure 1a - 1c.

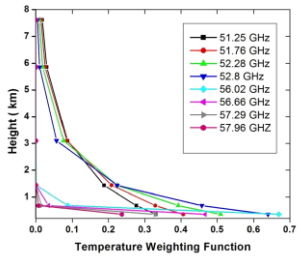

Figure 1a. Temperature weighting function at Fortaleza at 17.56UTC. The derived median values of daily radiosonde data are taken into consideration during the month April, 2011, for the purpose.

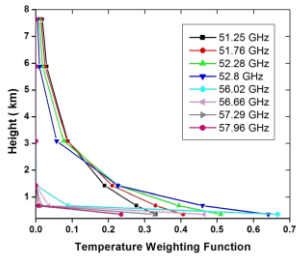

Figure 1b. Temperature weighting function at Belem at 17.33 UTC. The derived median values of daily radiosonde data are taken into consideration during the month June, 2011, for the purpose.

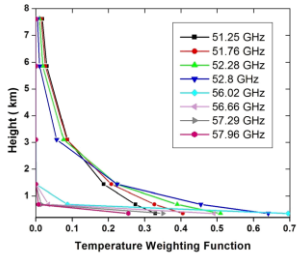

Figure 1c. Temperature weighting function at Alcantara at 17.57 UTC. The derived median values of daily radiosonde data are taken into consideration during the month March, 2010, for the purpose.

These figure show that the variation of brightness temperature with height occurs at 51 – 53 GHz but on the other hand the constancy of brightness temperature with height at 56 – 57 GHz is noticeable. This suggests that the measurement of temperature at a certain place by a ground based radiometer may provide good result by exploiting the 56 – 57 GHz band. In this band we have used four frequencies for the purpose. But to extend our study we have also made an attempt to retrieve the temperature profiles in 51 – 53 GHz band which will be presented in the subsequent sections.

IV. INVERSION TECHNIQUE

For the purpose of formulating the inverse problem in this particular context i.e., retrieving the temperature profile at three specified locations of Southern latitude we have purposely set the radiometer towards zenith, $\theta = 0$ direction. Hence, equation (2) can be rewritten retaining only the temperature term as

$$T_{DN}(h,f) = \int_0^\infty W_T(h,f)T(h)dh \quad (4)$$

Here, (refer to equation 4) the integral equation is linear in $T(h)$ assuming $W_T(h,f)$ is independent

of $T(h)$ .The non-linear form is not commonly encountered in the microwave region as it is in the infrared region. The infrared equivalent of the linear integral equation, for example, involves the Planck brightness function, which is strongly nonlinear in Temperature in the infrared region but is approximately linear for most of the microwave region. However, in practice $T(h)$ is usually measured at discrete number of frequencies, and the objective of the inversion technique is to find out a function $T(h)$ that, when substituted in equation (4) will give values of $T_{DN}(h,f)$ which might be approximately equal to the measured values [16]. If the integral of equation (4) is approximated as a summation over m layers each of height Δh , the radiometric temperature at frequencies f_i can be written as

$$T_{DN}(f) = \sum_{j=1}^{m} W(f_i h_j) T_{z_j} \quad (5)$$

Here, in our study, we have chosen four closely spaced frequencies 56 – 58 GHz in the lower shoulder of the 60 GHz oxygen spectrum and thereafter frequencies 51 – 53 GHz, for the purpose. For the sake of simplicity we write the equation (5) in a more compact form as

$$\boldsymbol{T_{DN}} = \boldsymbol{WT} \quad (6)$$

Where, $\boldsymbol{T_{DN}}$ and $\boldsymbol{T}$ are the vectors of dimension n and m respectively and $\boldsymbol{W}$ is an (n$\times m$) matrix.

The vector $\boldsymbol{T_{DN}}$ represents the observations; $\boldsymbol{W}$ is a weighting matrix also presumed known and $\boldsymbol{T}$ is the unknown atmospheric temperature profile. To get the good vertical resolution we have considered $m > n$. But with this idea, this will produce infinite number of solutions. Now to get rid of this issue i.e., to make the problem solvable we need *a priori* information about the character of the atmosphere for a given geographic location and a given time of year. This information includes the statistics about the temperature profile, constraints imposed by atmospheric physics, any other information that, if integrated into the inversion algorithm, would narrow the range of values that $T(h)$ can have. However, the degree of accuracy to which this information is incorporated in the inversion algorithm depends on the underlying structure of the variety of inversion method. Here, we have chosen the Optimal Estimation Method purposely for the retrieval method.

The a- priori (statistical) information, in the present context, is comprising of monthly averages of the vertical profiles of temperature and the constrains imposed by the atmospheres of particular places of Argentina, Brazil, China, Newzeland, India for the months July through August, 2005.

V. OPTIMAL ESTIMATION METHOD

We consider the brightness temperature as measured by the radiometer $\boldsymbol{T_{DN}}$ is linearly related to the unknown or sought function $\boldsymbol{g(h)}$. Then equation (6) can be written as

$$\boldsymbol{T_{DN}} = \boldsymbol{W g(h)} \quad (7)$$

where $\boldsymbol{T_{DN}}$ is the vector of order n and $\boldsymbol{g}$ is of order m and $\boldsymbol{W}$ is (n$\times m$) matrix and is commonly known as kernel or weighting function of the sought function $g(h)$. In practice we cannot measure the true $\boldsymbol{T_{DN}}$ exactly because of experimental error which may include both measurement error and modeling error. However, our main purpose is to achieve successful retrieval of an unknown vector $\boldsymbol{g}$ using observations $\boldsymbol{T_{DN}}$ with $m > n$. The key factor is to supplement the observations with sufficient *a priori* information for regularizing the ill-posed problem. This *a priori* information is the mean profile $\langle \boldsymbol{g} \rangle$ and its covariance matrix $\boldsymbol{S_g}$ where

$$\boldsymbol{S_g} = \langle \boldsymbol{g g'} \rangle \quad (8)$$

It is to be mentioned here that if $\boldsymbol{g}$ represents the atmospheric temperature profile $\boldsymbol{T(h)}$, then the representative ensemble of radiosonde measured temperature profiles can provide $\langle \boldsymbol{g} \rangle$ and its covariance $\boldsymbol{S_g}$. We also assume that the error vector $\in$ has a zero mean and is statistically independent of $\boldsymbol{g}$, but the error covariance matrix $\boldsymbol{S_\epsilon} = \langle \in \in' \rangle$ is known.

This optimal estimation method has the advantage of finding the most likely value of $\boldsymbol{g}$, based on the combination of *a priori* information $\langle \boldsymbol{g} \rangle$ and a real measurement through $\boldsymbol{T_{DN}}$ along with the associated covariance matrix. The optimal estimate of $\boldsymbol{g}$ may be obtained by generalizing the method to vectors as $\langle \boldsymbol{g} \rangle$ and $(\boldsymbol{DT_{DN}})$, where **D** is exact solution such that $\boldsymbol{WD = I}$, the identity matrix ([17]; [18]; [19]; [20]).
The solution of equation (6) is given by ([16])

$$g = \langle g \rangle + S_g W' \left(W S_g W' + S_\epsilon \right)^{-1} (T_{DN} - W\langle g \rangle) \quad (9)$$

VI. ANALYSES AND RESULTS

The relationship between the measurements, represented by the m- dimensional vector measurement $\boldsymbol{y}$, and the quantities to be retrieved, represented by the n – dimensional profile vector $\boldsymbol{x}$ may be expressed as

$$\boldsymbol{Y = F(X)} \quad (10)$$

This relationship is satisfied by infinite number of profile vectors for a finite particular set of y. Thus by applying inversion method to obtain an exact solution x, it must be constrained which is the statistical ensemble of a large number of historic radiosonde profiles as mentioned earlier. Now, the modification of equation (9) is done to get a better approximation and minimization of experimental error as well and is expressed as,

$$g' = < g > + S_g W' \left(W S_g W' + S_\epsilon \right)^{-1} (T_{DN} - W < g > - \gamma \times mean(< g > - g'')) \quad (11)$$

Here, $\boldsymbol{T_{DN}}$ contains both measurement errors and the errors originated due to the assumptions and approximations associated with models. The n X 1 matrices $< g >$,$\boldsymbol{g'}$, and $\boldsymbol{g''}$ denote the a- priori data set, retrieved temperature profile vector and radiosonde measurements respectively, being carried out at Fortaleza, Brazil on 11th April, 2011 at 05:39 and 17:36 UTC. A similar approach (as discussed earlier) being carried out using a- priori data set, radiometric measurements at specified frequencies and radiosonde measurements respectively, at Belem, Brazil on 26th June, 2011 at 05:30 UTC and on 17th June, 2011 at 17:33 UTC. And, following the modified equation (equation 11) of optimal estimation method, the entire measurements being repeated for Alcantara, Brazil on 12th March, 2010 at 06:03 UTC and on 15th March, 2010 at 17:57 UTC, so as to approximate and validate the model. Here, $\boldsymbol{S_g}$ is the mean and covariance matrix of $< g >$. $\boldsymbol{S_\epsilon}$ represents m X m error covariance matrix associated with m-dimensional radiometric observations. The Lagrangian Multiplier γ, is basically a positive real quantity to be determined empirically. Depending upon the band of frequencies and the time at which the observations were carried out, it can take up the values ranging from 1 to 200.
The profile vector representing statistical ensemble of temperature is a 6 X 1 matrix having elements exactly at the vertical coordinates of 0.351 km, 0.6866 km, 1.4327 km, 3.1005 km, 5.862 km and 7.613 km forming $< g >$. T_{DN} has 8 elements (1 x 8 matrix) each at the eight specified frequencies. For faithful analysis this 1 x 8 matrix is subdivided into two sub-ensembles each of (1 x4). The weighting functions associated with $< g >$ was calculated analytically. These weighting functions are then normalized to unit maxima for different frequencies separately. The experimental errors allied to radiometric observation forming 1 x 4 matrices for each segment, assuming zero mean error. These errors can be assumed rather easily and correctly by calculating the elements of $T_{DN} - W < g >$ corresponding to each radiometric observation and then finding their lowest possible ratio. The range of these errors lies within -1 to +1. The retrieval process starts with the calculations of S_g and S_ϵ for two sub-ensembles of radiometric observations separately. Here $\boldsymbol{S_g = \langle g g' \rangle}$ and $\boldsymbol{S_\epsilon = \langle \epsilon \epsilon' \rangle}$. The measured brightness temperatures at eight specified channel frequencies at Fortaleza, Brazil on 11th April, 2011 at 05:39 and 17:36 UTC are as shown in table 2. The summery of measured brightness temperature in oxygen band at Belem, Brazil on 26th June, 2011 at 05:30 UTC

and on 17th June, 2011 at 17:33 UTC and also at Alcantara, Brazil on 12th March, 2010 at 06:03 UTC and on 15th March, 2010 at 17:57 UTC are tabulated in table 3 and 4 respectively. The approximated results of temperature retrieval are shown from figure 2 to figure 7 separately for the three places of choice.

Table 2. Summary of Brightness Temperature Measured in Oxygen Band at Fortaleza

Date & Time	**Brightness Temperature in K**	**Frequency in GHz**							
		51.248	51.76	52.28	52.804	56.02	56.66	57.288	57.964
11/4/2011 5:39		124.092	140.774	166.392	199.965	293.843	294.943	295.669	296.053
11/4/2011 17:36		137.786	152.597	176.91	207.676	294.534	296.245	296.477	297.553

Table 3. Summary of Brightness Temperature Measured in Oxygen Band at Belem

Date & Time	**Brightness Temperature in K**	**Frequency in GHz**							
		51.248	51.76	52.28	52.804	56.02	56.66	57.288	57.964
26/6/2011 5:30		115.899	133.291	160.164	195.107	294.612	296.093	295.933	296.324
17/06/2011 17:33		124.305	141.799	167.661	200.014	296.673	297.739	299.324	299.718

Table 4. Summary of Brightness Temperature Measured in Oxygen Band at Alcantara

Date & Time	**Brightness Temperature in K**	**Frequency in GHz**							
		51.248	51.76	52.28	52.804	56.02	56.66	57.288	57.964
12/3/2010 6:03		123.084	136.897	162.706	198.142	296.006	296.065	296.852	297.793
15/3/2010 17:57		124.421	138.322	163.987	197.55	296.63	297.695	298.022	299.08

In Figures 2-7, we plot the statistical difference between retrieved air temperature profile using brightness temperatures measured by scanning radiometers and RAOBs measured air temperature profile, the mean value (BIAS), and the root mean square (RMS) of the difference between retrieved estimation and RAOBs measurements at the specified dates and times. Figure 3 shows highest air temperature profile retrieval accuracy comparable with the radiosonde observation being observed for Fortaleza, Brazil on 11th April, 2011 at 17:36 UTC. The RMS is smaller than 1.0 K up to 8 km; the only exception is around 6 km (1.5 K), while the BIAS does not exceed 0.7 K except around 6 km. While at Belem, Brazil, figure 5 clearly suggest that the highest air temperature profile retrieval accuracy comparable with the radiosonde observation found to be on 17th June, 2011 at 17:33 UTC. The RMS is smaller than 1.0 K up to 5 km and beyond this it is around 1.6 K, while the BIAS does not exceed ±1.0 K, except above 5 km (±1.3 K). A similar result is observed for Alcantara, Brazil on 15th March, 2010 at 17:57 UTC (Figure 7). The RMS is smaller than 1.0 K up to 8 km; the only exception is around 6 km (1.2 K), while the BIAS does not exceed ±0.6 K except around 6 km. On the other hand, in case of Fortaleza particularly, retrieval accuracy slightly degraded with observable RMS errors are varying with a maximum up to 2.5 K, while the BIAS does not exceed ±2.5 K on 11th April, 2011 at 17:36 UTC for retrieved profile (being derived with BT of lower frequency sub-ensemble). But it is effected by fairly high RMS (2.0 K to 6.0 K) and BIAS (-4.0-5.0 K) on 11th April, 2011 at 05:39 UTC (Figure 2). This is might be related to the temperature inversion around 0.7 km, but also to the lower surface temperature during local dawn time. While at Belem, Brazil we observed that the retrieval accuracy is affected by observably high RMS errors varies maximum up to 2.0 K and BIAS does not exceed ±1.6 K on 26th June, 2011 at 05:30 UTC (Figure 4). This is might be related to the fairly lower temperature difference between two subsequent layers near surface, during morning UTC. We noticed a similar result for Alcantara with retrieval accuracy is effected by fairly high RMS (1.0 K to 2.0 K) and BIAS (-1.5-1.5 K) on 12th March, 2010 at 06:03 UTC (Figure 6). This observation is also valid for the retrieved profile when derived using the brightness temperatures of

lower frequency sub-ensemble. The following figures show the comprehensive inaccuracies happen at 05:39 UTC. Statistics confirm that at Fortaleza as well as Alcantara, the results are in good agreement during afternoon when the retrieval method being carried out with the brightness temperatures for upper frequency sub-ensembles. But this is partly supported by the results at Belem. Here also statistically fairly high accuracy being observed during afternoon Universal Time Coordinates [UTC], when the retrieval method is being carried out not only with the brightness temperatures for upper frequency sub-ensemble but also with the BTs of lower frequency channels in the oxygen band separately.

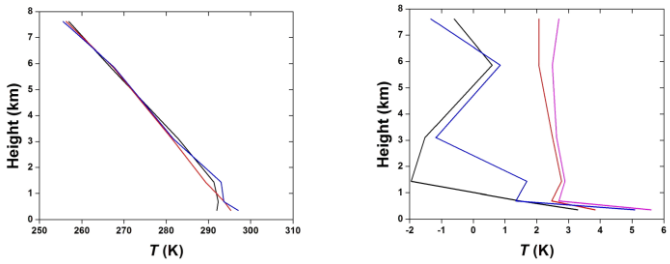

(a) (b)

Figure 2. Statistical difference between retrieved air temperature profiles when retrieved with BTs of two frequency sub-ensembles separately and temperature profile measured by RAOBs for Fortaleza, Brazil on 11th April, 2011 at 05:39 UTC are shown in red (upper frequencies), blue (lower channels) and black respectively (a). The corresponding measured BIAS is shown in black and blue; while the RMS is shown in red and magenta, while retrieved using BTs measured for both upper and lower frequency sub-ensembles respectively (b).

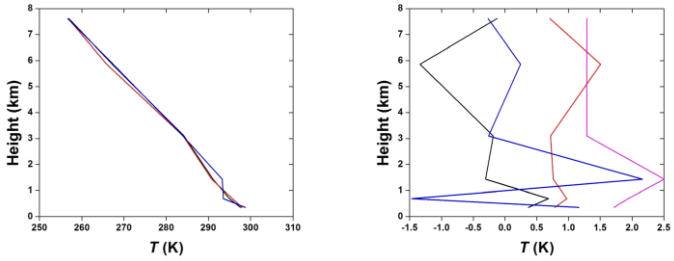

(a) **(b)**

Figure 3. Statistical difference between retrieved air temperature profiles when retrieved with BTs of two frequency sub-ensembles separately and temperature profile measured by RAOBs for Fortaleza, Brazil on 11th April, 2011 at 17:36 UTC are shown in red (upper frequencies), blue (lower channels) and black respectively (a). The corresponding measured BIAS is shown in black and blue; while the RMS is shown in red and magenta, while retrieved using BTs measured for both upper and lower frequency sub-ensembles respectively (b).

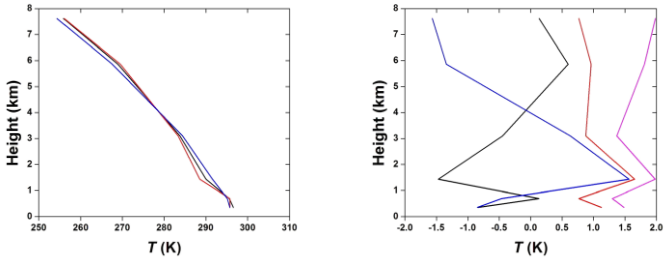

(a) (b)

Figure 4. Statistical difference between retrieved air temperature profiles when retrieved with BTs of two frequency sub-ensembles separately and temperature profile measured by RAOBs for Belem, Brazil on 26th June, 2011 at 05:30 UTC are shown in red (upper frequencies), blue (lower channels) and black respectively (a). The corresponding measured BIAS is shown in black and blue; while the RMS is shown in red and magenta, while retrieved using BTs measured for both upper and lower frequency sub-ensembles respectively (b).

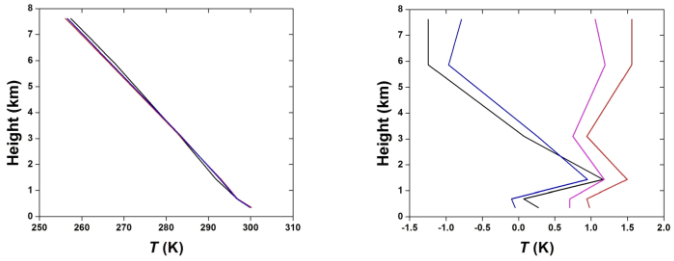

(a) (b)

Figure 5. Statistical difference between retrieved air temperature profiles when retrieved with BTs of two frequency sub-ensembles separately and temperature profile measured by RAOBs for Belem, Brazil on 17th June, 2011 at 17:33 UTC are shown in red (upper frequencies), blue (lower channels) and black respectively (a). The corresponding measured BIAS is shown in black and blue; while the RMS is shown in red and magenta, while retrieved using BTs measured for both upper and lower frequency sub-ensembles respectively (b).

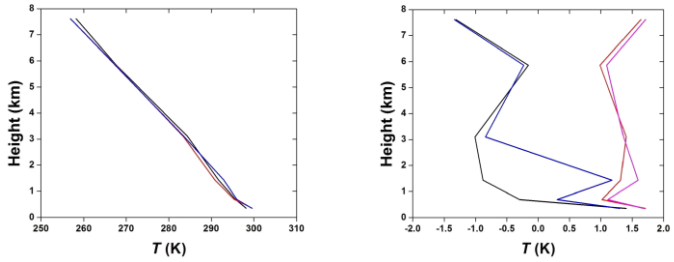

(a) (b)

Figure 6. Statistical difference between retrieved air temperature profiles when retrieved with BTs of two frequency sub-ensembles separately and temperature profile measured by RAOBs for Alcantara, Brazil on 12th March, 2010 at 06:03 UTC are shown in red (upper frequencies), blue (lower channels) and black respectively (a). The corresponding measured BIAS is shown in black and blue; while the RMS is shown in red and magenta, while retrieved using BTs measured for both upper and lower frequency sub-ensembles respectively (b).

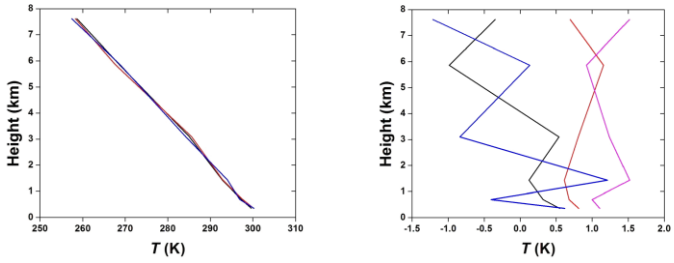

(a) (b)

Figure 7. Statistical difference between retrieved air temperature profiles when retrieved with BTs of two frequency sub-ensembles separately and temperature profile measured by RAOBs for Alcantara, Brazil on 15th March, 2010 at 17:57 UTC are shown in red (upper frequencies), blue (lower channels) and black respectively (a). The corresponding measured BIAS is shown in black and blue; while the RMS is shown in red and magenta, while retrieved using BTs measured for both upper and lower frequency sub-ensembles respectively (b).

VII. DISCUSSIONS AND CONCLUSIONS

The optimal estimation method is a kind of method that combines the observations with a background taken from numerical weather prediction (NWP) model outputs. The assumed error characteristics of both are taken into account ([21]). However, the 1DVAR approach (One- Dimensional Variation Technique was demonstrated to be advantageous over methods using background from statistical climatology ([22]). In fact, as background information, 1DVAR uses a forecast state vector, which is usually more representative of the actual state than a climatologic mean. A comparative analysis

between a variety of retrieval methods applied to ground-based observations from conventional microwave radiometers (such as MWRP) indicated that the 1DVAR technique outperforms the other considered methods, these being based on various kinds of multiple regression and neural network. Thus, it seemed convenient to couple the sensitivity of millimetre-wave radiometry with the advantages of the 1DVAR technique for the retrieval of temperature and humidity profiles [23]. While developing this technique the standard notation is used as used by [24] and indicated with B and R the error covariance matrices of the background and observation vector y, respectively. In addition, the forward-model operator (i.e., radiative transfer model) with F(**x**) was used. Thus, the technique adjusts the state vector x from the background state vector $X_b$to minimize the following cost function

$$J = [y - F(X)]^T R^{-1}\left[y - F(X) + (X - X_b)^T B^{-1}[X - X_b]\right] \quad (12)$$

Here T and -1 represents the matrix transpose and inverse. The radiometric noise, representativeness, and forward-model errors all contribute to the observation-error covariance R. The minimization is achieved using the Levemberg–Marquardt method; this method was found to improve the convergence rate with respect to the classic Gauss–Newton method ([21]) by introducing a factor γ that is adjusted after each iteration depending on how the cost function *J* has changed; thus, calling K the Jacobian matrix of the observation vector with respect to the state vector, the solution

$$X_{i+1} = X_i + [(1+\gamma)B^{-1} + K_i^T R^{-1} K_i]^{-1}.[K_i^T R^{-1}(y - F(X_i) - B^{-1}(X_i - X_B)] \quad (13)$$

is iterated until the following convergence criterion is satisfied

$$[F(X_{i+1}) - F(X_i)]^T S^{-1}[F(X_{i+1}) - F(X_i)] \ll N \text{ (Observations)} \quad (14)$$

Here, $S = R(R + K_i B K_i^T)^{-1}R$ and N(Obs.) indicates the number of observations (i.e., the dimension of **y**).

The GSR was first deployed during the Water Vapour Intensive Operational Period (WVIOP, March–April 2004) and, later, during the Radiative Heating in Underexplored Bands Campaign (RHUBC, February–March 2007), both held at the Atmospheric Radiation Measurement (ARM) Program's North Slope of Alaska (NSA) site in Barrow, Alaska ([25]).

The state vectors that used by [23] are profiles of temperature and total water (i.e., total of specific humidity and condensed-water content ([26]). The choice of total water has the advantages of reducing the dimension of the state vector, enforcing an implicit correlation between humidity and condensed water, including a super-saturation constraint. Moreover, the introduction of natural logarithm of total water creates error characteristics that are more closely Gaussian and prevents unphysical retrieval of negative humidity. The background-error covariance matrices B for both temperature and humidity profiles may be computed from a set of simultaneous and co-located forecast-RAOB data (both in clear and cloudy conditions). This calculation of B inherently includes forecast errors as well as instrumental and representativeness errors from the radiosondes. The radiosonde instrumental error is assumed to be negligible compared with the representativeness error, which consists of the error associated with the representation of volume data (model) with point measurements (radiosondes). The B matrix including these terms seems appropriate for the radiometric retrieval minimization; since the grid cell of the NWP model is much larger than the radiometer observation volume, the latter can be assumed as a point measurement compared with the model cell, similar to radiosondes. It may be assumed that the B matrix estimated for humidity to be valid for control variable total water, since no information on the background cloud-water error covariance was available. This assumption is strictly valid during clear sky conditions only, while it underestimates the background error in cloudy conditions. The implications are that, under cloudy conditions, humidity retrieval would rely more on the background and less on measurements than would be possible by adopting a B matrix that includes both humidity and liquid-water errors. However, considering the infrequent and optically thin cloudy conditions encountered during RHUBC, it is understood that this assumption does not affect results significantly.

The observation vector is defined as the vector of $T_B$measured by GSR at a number of elevation angles, plus the surface temperature and humidity given by the sensors mounted on the lowest level

(2m) of the meteorological tower. The observation error covariance matrix R may be estimated using the GSR data taken from the WVIOP, following the approach by [21]. The forward model $F(X)$ is provided by the NOAA microwave radiative-transfer code ([27])which also provides the weighting functions that were used to compute the Jacobians K with respect to temperature, humidity, and liquid water. The typical errors with respect to band-averaged $T_B$are within 0.1 K and were accounted for in the forward-modelling component of the observation error.

The 1DVAR retrieval technique and the settings described in the previous section were applied to GSR data collected during the three-week duration of RHUBC. These observations were found to be consistent with simultaneous and co-located observations from the other two independent 183-GHz radiometers and with simulations obtained from RAOBOs ([28]), generally within the expected accuracy. As a comparison, the background NWP profiles were shown that were used as a first guess and the *in situ* observations from the radiosonde.

Concerning the temperature profile, it is noted that in this case, the NWP forecast is in good agreement with the RAOB, particularly in the atmospheric layer from 0.5 to 3.0 km. Conversely, in the upper part of the vertical domain (3–5 km), the NWP forecast shows about 1–2-K bias with respect to the RAOB, while in the very first layer (0–0.5 km), it differs from RAOB by more than 10 K. Conversely, the 1DVAR retrieval agrees better with the RAOB in the lowest levels, while for the upper levels, the retrieved temperature tends to lie over the NWP background.

As for the humidity, again it is noted that the NWP forecast captures well the vertical structure, although with lower resolution, except for the first 500 m, where the 1DVAR retrieval shows a much better agreement with the RAOB.

The analyses show that at Fortaleza, the upper frequency band i.e., 56-58 GHz consisting of four frequency channels built in the said radiometer provides a good agreement regarding temperature profiling, with the RAOB's. But on the other hand, at Belem the lower frequency band i.e., 51-53 GHz consisting of four frequency channels built in the said radiometer provides a good agreement regarding temperature profiling, with the RAOB's. It may also be noted that at Alcantara, the lower frequency band show good agreement, in this regard. All these agreement happen to be good during afternoon and the situation is worst during midnight (UTC). It is also observed that as we move towards the higher latitude the possibility of getting good agreement with RAOB's upper air data lies in favor of using the higher frequency channels.

VIII. FUTURE SCOPE

In future we are very much interested to use others retrieval method such as Backus Gilbert Synthetic Averaging Inversion method, neural network method etc. for retrieval of vertical profiles of atmospheric temperature over the aforesaid three places choice and try to find out the most suitable and simplified inversion method for retrieving of atmospheric temperature profile both in terms of accuracy and resolution with minimal operating and instrumental limitations. In future, using the potentials offered by ground-based multichannel microwave radiometry we are very much interested to apply the Modified Optimal Estimation Method for continuous vertical profiling of humidity as well as water vapour in order to validate the model.

REFERENCES

[1].Solheim, F., Godwin, J. R., Westwater, E.R., Han,Y., Keihm, S. J., Marsh, K., Ware, R., (1998) "Radiometric profiling of temperature, water vapor and cloud liquid water using various inversion methods", Radio Science, Vol. 33, No. 2, pp 393-404.

[2].Westwater, E. R., Crewell, S., Matzler, C., (2004) "A Review of Surface-based Microwave and Millimeter wave Radiometric Remote Sensing of the Troposphere", URSI Radio Science Bulletin, No. 310, pp 59-80.

[3].Rocken,C., Johnson, J. M., Neilan, R. E., Cerezo, M., Jordan , J. R., Falls, M. J., Nelson , L. D., Ware, R. H., Hayes, M., (1991) "The Measurement of Atmospheric Water Vapor: Radiometer Comparison and Spatial Variations", IEEE Transactions on Geoscience and Remote Sensing, Vol. 29, Issue 1, pp 3-8.

[4].Westwater, E.R., (1993) Ground-based Microwave Remote Sensing of Meteorological Variables, in: Michael A. Janssen (Eds.), Atmospheric Remote Sensing by Microwave Radiometry. J. Wiley & Sons, Inc. (New York), pp.145-213.

[5].Westwater, ED R., Han, Y., Solheim, F., (2000) Resolution and accuracy of a multi-frequency scanning radiometer for temperature profiling, in: P. Pampaloni and S. Paloscia (Eds.), Microwave Radiometry and Remote Sensing of the Earth's Surface and Atmosphere. VSP 2000 (Netherland), pp. 129-135.
[6].Ware, R., Solheim , F., Carpenter, R., Gueldner, J., Liljegren, J., Nehrkorn, T., Vandenberghe, F., (2003) "A multichannel radiometric profiler of temperature, humidity and cloud liquid", Radio Science, Vol. 38, No. 4, 8079, pp 4401-4413.
[7].Karmakar, P. K., Maiti, M., Sett, S., Angelis, C. F., Machado, L.A.T., (2011a) "Radiometric Estimation of Water Vapor Content over Brazil", Advances in Space Research, Vol. 48, No. 9, pp 1506-1514.
[8].Karmakar, P. K., Maiti, M., Calheiros, A.P.J., Angelis, C.F., Machado, L.A.T., Da Costa, S.S., (2011 b) "Ground based single frequency microwave radiometric measurement of water vapour", International Journal of Remote Sensing, Vol. 32, No. 23, pp 8629-8639.
[9].Mondal, S., Pradhan, A.K., Karmakar, P.K., (2014) "water vapour profiling at southern latitudes by deploying microwave radiometer", International Journal of Advances in Engineering & Technology, Vol. 6, Issue 6, pp 2646-2656.
[10].Karmakar, P.K., (2013) Ground-Based microwave radiometry and remote sensing, CRC press, Boca Raton, FL (USA), pp 224.
[11].Askne, J. I. H., Westwater, E. R., (1986) "A Review of Ground-Based Remote Sensing of Temperature and Moisture by Passive Microwave Radiometers", IEEE Transactions on Geoscience and Remote Sensing, GE-24(3), pp 340-352.
[12].Canavero, F. G., Einaudi, F., Westwater , E. R., Falls, M. J., Schroeder, J. A., Bedard Jr, A. J., (1990) "Interpretation of ground-based radiometric observations in terms of a gravity wave model", Journal of Geophysical Research, Vol. 95, No. D6, pp 7637-7652.
[13].Goody, R. M., Yung, Y. L., (1995). Atmospheric Radiation: Theoretical Basis, 2nd Edition, Oxford University Press (USA).
[14].Gasiewski, A. J., (1993) Microwave Radiative Transfer in Hydrometeors, in: Michael A. Janssen (Eds.), Atmospheric Remote Sensing by Microwave Radiometry. J. Wiley & Sons, Inc (New York), pp.1-36.
[15].Westwater, Ed. R., Crewell, S., Matzler, C., Cimini, D., (2005) "Principles of Surface-based Microwave and Millimeter wave Radiometric Remote Sensing of the Troposphere", Quaderni Delle Societa Italiana Di Elettromagnetismo, Vol. 1, No. 3, pp 50-90.
[16].Ulaby, F. T., Moore, R. K., Fung, A. K., (1986) Microwave Remote Sensing-Active and Passive, vol. 3, Artech House, Inc. (Norwood).
[17].Cimini, D., Shaw, J. A., Han, Y., Westwater, E. R., Irisovi, V., Leuski, V., Churnside, J. H., (2003) "Air Temperature Profile and Air-Sea Temperature Difference Measurements by Infared and Microwave Scanning Radiometers", Radio Science, Vol. 38, No. 3, 8045, pp 1001-1019.
[18].Westwater, E. R., Snider, J. B., Carlson, A. C., (1975) "Experimental Determination of Temperature Profiles by Ground-Based Microwave Radiometry", Journal of Applied Meteorology, Vol. 14, No. 4, pp 524-539.
[19].Rodgers, C. D., (1976) "Retrieval of Atmospheric Temperature and Composition from Remote Measurement of Thermal Radiation", Reviews of Geophysics, Vol. 14, No. 4, pp 609-624.
[20].Rodgers, C. D., (2000) Inverse Methods for Atmospheric Sounding: Theory and Practice, i-xvi. World Scientific Publishing (Singapore).
[21].Hewison, T., (2007) "1D-VAR retrievals of temperature and humidity profiles from a ground-based microwave radiometer", IEEE Transactions on Geoscience and Remote Sensing, Vol. 45, No. 7, pp 2163–2168.
[22].Cimini, D., Hewison, T. J., Martin, L., Güldner, J., Gaffard, C., Marzano, F. S., (2006) "Temperature and humidity profile retrievals from groundbased microwave radiometers during TUC", Meteorology Z., Vol. 15, No. 5, pp 45–56.
[23].Cimini, D., Westwater, Ed R., Gasiewski, A. J., (2010) "Temperature and Humidity Profiling in the Arctic Using Ground-Based Millimeter-Wave Radiometry and 1DVAR", IEEE Transactions on Geoscience and Remote Sensing, Vol. 48, No. 3, pp 1381-1388.
[24].Ide, K., Courtier, P., Ghil, M., Lorenc, A. C., (1997) "Unified notation for data assimilation: Operational, sequential, and variational", Journal of Meteorological Society of Japan, Vol. 75, No. 1B, pp 181–189.
[25].Ackerman, T. P., Stokes, G. M., (2003) "The atmospheric radiation measurement program", Physics Today, Vol. 56, No. 1, pp 38–44.
[26].Deblonde, G., English, S., (2003) "One-dimensional variational retrievals for SSMIS simulated observations", Journal of Applied Meteorology, Vol. 42, No. 10, pp 1406–1420.
[27].Schroeder, J. A., Westwater, E. R., (1991) User's guide to WPL microwave radiative transfer software, Nat. Ocean. Atmos. Admin., Boulder, CO, NOAA Technical Memorandum, ERL WPL-213.
[28].Cimini, D., Nasir, F., Westwater, E. R., Payne, V. H., Turner, D. D., Mlawer, E. J., Exner, M. L., Cadeddu, M. P., (2009) "Comparison of ground based millimeter-wave observations and simulations in the Arctic winter", IEEE Transactions on Geoscience and Remote Sensing, Vol. 47, No. 9, pp 3098–3106.

AUTHORS

Ayan Kanti Pradhan (b. 1980) is an M.Sc. of the Vidyasagar University, West Bengal, India and currently pursuing his research work under the supervision of Dr. Pranab Kumar Karmakar in the Department of Radiophysics & Electronics, University of Calcutta. His field of research includes vertical profiling and estimation of atmospheric constituent's especially ambient temperature deploying ground based microwave radiometer as well as employing Radiosonde data.

Since 2010, till date he acted as Assistant Professor in the Department of Electronics, Acharya Prafulla Chandra College, West Bengal, India, where he is involved in teaching in both the Post-graduate and under-graduate classes in areas such as microwave devices, communication, control system and instrumentation.

Subrata Mondal (b. 1984) received the B-Tech degree in Electronics & Communication Engineering from Murshidabad College of Engineering & Technology, W.B.U.T in 2007 and M-Tech degree in Radiophysics & Electronics from Institute of Radiophysics & Electronics, C.U in 2009. He is currently working as an Assistant professor in the department of Electronics & Communication Engineering at Dumkal Institute of Engineering and Technology, W.B.U.T and pursuing research work leading to PhD degree under the supervision of Dr. P.K. Karmakar at Institute of Radiophysics & Electronics, C.U., India.

He taught courses on electromagnetics, remote sensing and wave propagation theory. His technical interest include passive and active remote sensing, radiative transfer, microwave engineering.

Pranab Kumar Karmakar is currently pursuing his research work basically in the area of modeling of integrated water vapour and liquid water in the ambient atmosphere. Ground based microwave radiometric remote sensing is his special area of interest. This includes the vertical profiling of thermodynamic variables. He is presently involved in the research and teaching in the Post-graduate classes of Institute of Radiophysics and Electronics, University of Calcutta.

Since his joining in 1988 in the University of Calcutta, India, Dr. Karmakar published his noteworthy outcomes of researches over tropical locations in different international and national journals of repute. All these are culminated into a book entitled Microwave Propagation and Remote Sensing: Atmospheric Influences with models and Applications published by CRC Press in 2012.

He had been awarded the International Young Scientist award of URSI in 1990. Also, he had been awarded the South-South Fellowship of TWAS in 1997. He acted as visiting scientist in Remote Sensing Laboratory, University of Kansas, USA; Centre for Space Sciences, China, and National Institute for Space Sciences, Brazil.